ACS APPLIED MATERIALS & INTERFACES

Research Article

www.acsami.org

Surface-Independent Antibacterial Coating Using Silver Nanoparticle-Generating Engineered Mussel Glue

Yun Kee Jo,[†,§] Jeong Hyun Seo,[†,‡,§] Bong-Hyuk Choi,[†] Bum Jin Kim,[†] Hwa Hui Shin,[†] Byeong Hee Hwang,[†] and Hyung Joon Cha*[,†]

[†]Department of Chemical Engineering, Pohang University of Science and Technology, Pohang 790-784, Korea

[‡]School of Chemical Engineering, Yeungnam University, Gyeongsan 712-749, Korea

Supporting Information

ABSTRACT: During implant surgeries, antibacterial agents are needed to prevent bacterial infections, which can cause the formation of biofilms between implanted materials and tissue. Mussel adhesive proteins (MAPs) derived from marine mussels are bioadhesives that show strong adhesion and coating ability on various surfaces even in wet environment. Here, we proposed a novel surface-independent antibacterial coating strategy based on the fusion of MAP to a silver-binding peptide, which can synthesize silver nanoparticles having broad antibacterial activity. This sticky recombinant fusion protein enabled the efficient coating on target surface and the easy generation of silver nanoparticles on the coated-surface under mild condition. The biosynthesized silver nanoparticles showed excellent antibacterial efficacy against both Gram-positive and Gram-negative bacteria and also revealed good cytocompatibility with mammalian cells. In this coating strategy, MAP-silver binding peptide fusion proteins provide hybrid environment incorporating inorganic silver nanoparticle and simultaneously mediate the interaction of silver nanoparticle with surroundings. Moreover, the silver nanoparticles were fully synthesized on various surfaces including metal, plastic, and glass by a simple, surface-independent coating manner, and they were also successfully synthesized on a nanofiber surface fabricated by electrospinning of the fusion protein. Thus, this facile surface-independent silver nanoparticle-generating antibacterial coating has great potential to be used for the prevention of bacterial infection in diverse biomedical fields.

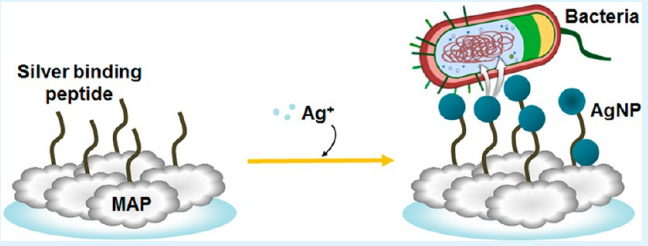

KEYWORDS: *antibacterial coating, mussel adhesive protein, silver binding peptide, silver nanoparticle, surface-independent coating*

INTRODUCTION

Bacterial infections cause critical complications in the initial stages of orthopedic and dental surgeries.[1] Once bacteria attach to implantable materials or devices, consecutive processes occur that ultimately lead to biofilm formation. Thus, the demand for antibacterial agents, which prevent bacterial infection by preventing primary bacterial attachment or by killing bacteria,[2−4] has continued to increase. Metal nanoparticles have been considered to be highly promising antibacterial agents because of their outstanding physical, chemical, and biological properties, which are provided by their large active surface area,[5,6] and studies on metal nanoparticles have been followed by recent advances in the field of nanotechnology.[7] These advances include the development of silver nanoparticles that release silver ions and show broad antibacterial activity against both Gram-positive and Gram-negative bacteria, including highly multiresistant strains such as methicillin-resistant *Staphylococcus aureus* (MRSA).[8,9] In addition, various surface functionalization methods for immobilization of silver nanoparticles have also been studied to ensure appropriate level of biological safety as well as antibacterial activity.[10,11] Thus, biomedical materials incorporating silver nanoparticles have been devised, including catheters, dental materials, and medical devices[12] using chemical or physical method.[13] However, the synthesis of silver nanoparticles by chemical or physical method needs surfactant and stabilizer to prevent unwanted agglomeraion.[14] These chemicals, which may remain as contaminants in the final product, are often toxic.[15]

Silver binding peptides, which are capable of inducing the formation of silver nanoparticles in a solution of $AgNO_3$, have been identified by phage display technology.[16,17] These peptides have specific affinity to silver ions and induce silver biomineralization, which promotes the reduction of silver ions by mimicking the recognition and nucleation capabilities found in biomolecules for inorganic silver material synthesis.[18−20] It was known that peptide-based synthesis can control shape, size, and size distribution of silver nanoparticles.[21] In addition, the synthesis occurs under relatively mild condition and does not require environmentally toxic chemicals such as surfactant and stabilizer.[22] Furthermore, silver binding peptide acts as a reducing agent and a stabilizer and does not require additional step for reducing and stabilizing the synthesized nano-

Received: August 27, 2014
Accepted: October 14, 2014
Published: October 14, 2014

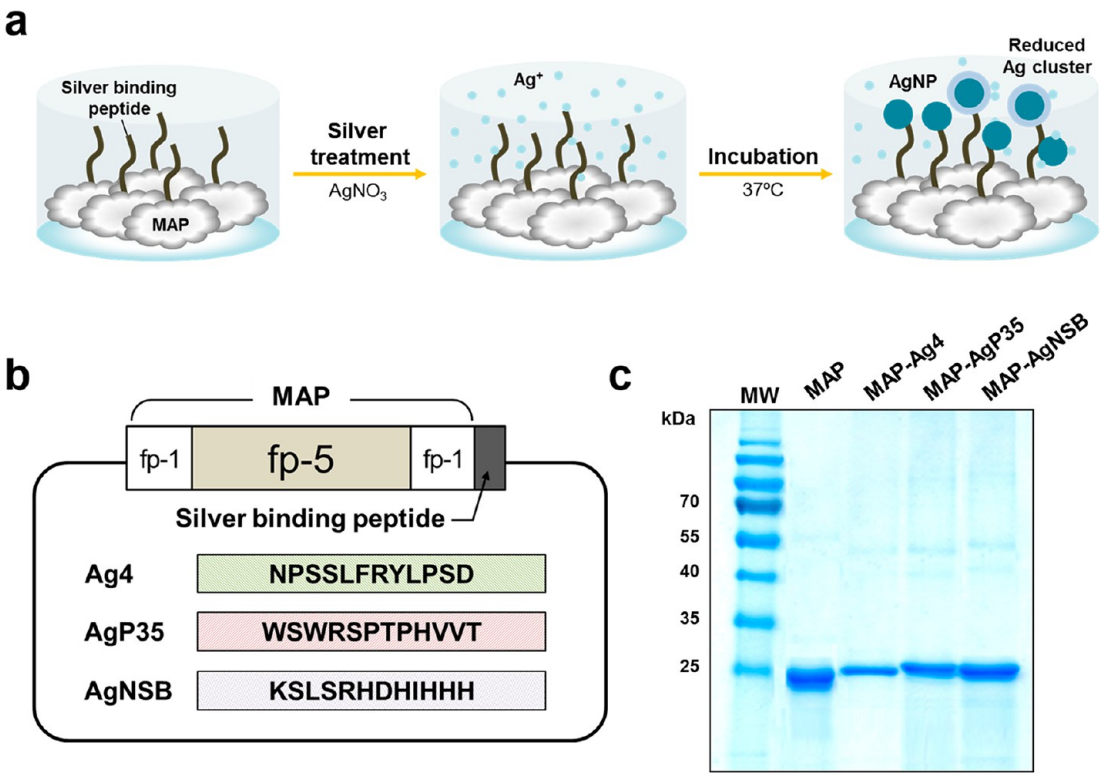

Figure 1. Silver nanoparticle synthesis process and construction of MAP-silver binding peptide fusions. (a) Diagram of the MAP-based silver nanoparticle synthesis process. (b) Diagram of vector construction for MAP-silver binding peptide fusions. (c) SDS-PAGE analysis of purified MAP-silver binding peptide fusions.

particles.[23,24] However, the simple mixing of peptides and $AgNO_3$ liquid solutions could bring many drawbacks, including poor attachment of the silver nanoparticles on target surface. Even though the immobilization of silver binding peptides has been attempted, their methods were only targeted on limited matrices such as polymer film and chitosan scaffold by simple mixing.[25,26] Previsouly, various approaches have been reported for the preparation of silver nanoparticles via catechol oxiation of DOPA or DOPA analogues (e.g., dopamine)-based materials,[27−29] but these methods did not include incorporation of silver binding peptides. Thus, advanced strategies are needed to immobilize the silver binding peptides and/or silver nanoparticles effectively on various surface types for practical use.

Mussel adhesive proteins (MAPs) are promising bioadhesives derived from the marine mussel to be used in various tissue engineering and medical applications because of their unique properties, such as superior adhesion, water resistance, biocompatibility, and biodegradability.[30,31] In particular, MAPs adhere to various surfaces, such as plastic, glass, metal, and leather, with great adhesion strength. Previously, a recombinant hybrid-type MAP was successfully designed and expressed in a bacterial system with high production and purification yields.[32] Recombinant MAPs can easily be fused with different short functional peptides, thus enabling different biological functions and providing adhesion properties for tissue engineering applications without any additional surface modification steps.[33,34] Moreover, recombinant MAPs could easily be fabricated to various forms such as nanofiber and coacervate.[35,36]

In the present study, we exploited a simple method for surface-independent antibacterial coating by constructing a recombinant MAP fused with functional silver binding peptide and reducing silver nanoparticles on the fusion protein-coated surface. MAP-silver binding peptide fusion proteins could coat on any surface types with strong adhesion ability, thus providing silver binding moieties as templates for silver nanoparticle synthesis on target surface under mild condition without using any additional reducing agents or stabilizers. In hybrid biomaterials made this way, MAP-silver binding peptide fusion proteins nucleate and control the growth of silver nanoparticle as organic templates, while inorganic silver nanoparticles present antibacterial activities. Figure 1a shows that MAP-silver binding peptide fusion proteins adsorb silver ions in aqueous $AgNO_3$ and attach them to the target material surface. They, then, reduce the silver ions to form silver nanoparticles. As we demonstrated in this scheme, this work was to propose a new biomaterial for efficient surface-independent coating that has high adhesive strength and high antibacterial activity, achieved through the combination of silver nanoparticles and MAP.

MATERIALS AND METHODS

Construction of Expression Vectors. We designed a forward primer based on the N-terminal sequence of hybrid-type MAP fp-151 and reverse primers that incorporate the silver binding peptide sequences identified by the phage display (Supporting Information Table S1).[16] The pET-22b(+) vector (Novagen) containing the T7 promoter was used for expression of the fusion proteins in *Escherichia coli* BL21 (DE3) (Novagen). Ligated vectors were transformed into *E. coli* TOP10 (Invitrogen), which was the host used for gene cloning, and the transformed cells were grown in Luria−Bertani

(LB) medium with 50 μg mL^{-1} ampicillin (Sigma). All cloned sequences were verified by direct sequencing.

Expression and Purification of MAP-Silver Binding Peptide Fusions. To express the different MAP-silver binding peptide fusion proteins, we transformed the recombinant vectors into *E. coli* BL21 (DE3), and the cells were cultured in LB medium with 50 μg mL^{-1} ampicillin at 37 °C and 300 rpm. At a 600 nm optical density (OD_{600}) of 0.4−0.6, 1 mM isopropyl-β-D-thiogalactopyranoside (IPTG; Sigma) was added to the culture broth to induce protein expression, and the cells were grown for 8 h at 37 °C and 300 rpm. After harvesting by centrifugation of the culture broth at 18 000*g* for 10 min at 4 °C, the cells were resuspended in 5 mL lysis buffer (10 mM Tris-HCl and 100 mM sodium phosphate; pH 8.0) per gram wet weight, and they were lysed using a cell disruption system (Constant Systems) at 20 Kpsi. The cell lysates were centrifuged at 18 000*g* and 4 °C for 20 min to collect cell debris, and the fusion proteins were extracted by using 25% (v/v) acetic acid. Purified proteins were freeze-dried and stored at −80 °C. The expression and purification of each sample were analyzed by 12% (w/v) sodium dodecyl sulfate-polyacrylamide gel electrophoresis (SDS-PAGE), and protein concentrations were determined by the Bradford assay (Bio-Rad), with bovine serum albumin (BSA; Promega) as the protein standard.

Surface Coating of MAP-Silver Binding Peptide Fusions. Transparent polystyrene coverslips (SPL Life Science) with a thickness of 0.11 mm and a diameter of 9 mm that do not affect absorption in UV−vis spectroscopic analyses were used as sample surfaces. The sample surfaces were first incubated in original MAP or MAP-silver binding peptide fusions in distilled water (DW) at a 3 mg mL^{-1} concentration for 30 min. After the solution was dispensed onto the surface using a spin coater (Jaeseong) at 1000 rpm for 10 s and 3000 rpm for 20 s sequentially, the surface was washed in DW to remove excess and loosely tethered original MAP or MAP-silver binding peptide fusions. MAP was spin-coated to be spread uniformly and widely onto surfaces, although it could be coated in various ways such as simple dipping and adsorption.[32−34] A bare polystyrene coverslip surface was used as a negative control, and the original MAP-coated surface was used as a comparative control.

Formation of Silver Nanoparticles. The surfaces coated with MAP-silver binding peptide fusions were incubated with 20 mM $AgNO_3$ solution for up to 6 days. After incubation, loosely attached silver nanoparticles were removed by washing with DW. UV−vis spectroscopic analysis was used to monitor the formation of silver nanoparticles in a microplate reader (PerkinElmer); the absorbance in the range of 390−550 nm was measured. The morphology of the silver nanoparticles formed on $AgNO_3$-treated surfaces was analyzed using field emission-scanning electron microscopy (FE-SEM; Philips) after Pt-coating using a sputter coater (Paraone). Elemental analyses were performed using energy dispersion X-ray spectroscopy (EDS; Genesis system) and X-ray photoelectron spectroscopy (XPS; VG Scientific).

Control of Silver Nanoparticle Formation. To investigate the effect of incubation time with $AgNO_3$ solution on silver nanoparticle formation, the MAP-Ag4-coated polystyrene surface was incubated for 8 days with 1 day interval. The effect of MAP-silver binding peptide fusion concentration in coating solution was examined by varying protein concentration (1, 3, 5, and 10 mg mL^{-1}). Morphologies of surface-formed silver nanoparticles were analyzed using SEM.

Silver Release Profile. The amount of silver release from the MAP-Ag4-coated polystyrene surface was determined by inductively coupled plasma-optical emission spectroscopy (ICP-OES; Thermo). The surface was immersed in 500 μL of phosphate-buffered saline (PBS; HyClone) for 1 day in dark, and then the PBS solution containing released silver was collected. The surface was immersed again in fresh PBS and this process was repeated every day for 7 days. For ICP-OES analysis, PBS was diluted with 5% (v/v) HNO_3 solution and the standard was prepared using an ICP standard Ag solution (AnApure).

Antibacterial Activity Test. To examine the antibacterial activity of the silver nanoparticles, we used the Kirby−Bauer method.[37] MAP-silver binding peptide fusions-coated polystyrene coverslips with silver nanoparticles were placed on LB agar plates having log-phase-grown bacterial cells, and incubated overnight at 37 °C. The Gram-negative bacteria *E. coli* (ATCC 25922), *Salmonella enterica* subspecies *enterica* serotype Typhimurium (IFO 12529), and *Shigella dysenteriae* (ATCC 13313) and the Gram-positive bacterium *Staphylococcus aureus* (ATCC 6538) were used. The diameter of the inhibition zone was measured in triplicate using calipers. To determine growth curves in the presence of silver nanoparticles produced by MAP-silver binding peptide fusions, $AgNO_3$-treated surfaces were incubated in 500 μL of LB medium inoculated with 5 μL of the log-phase culture of each bacterial strain.

In addition, the silver nanoparticle-formed surfaces were incubated with 1×10^9 cells mL^{-1} of *E. coli* in 500 μL of LB media in 48-well culture plates (SPL Life Science) to evaluate bactericidal activity. The cells that contacted the $AgNO_3$-treated surfaces were incubated at 37 °C and 300 rpm. Bacterial concentrations and growth/death rates were monitored by measuring OD_{600} for a 24 h period.

Sustainability Test. The sustainability of silver nanoparticles on the MAP-Ag4-coated polystyrene surface was evaluated by antibacterial activity assays for 7 days. To determine growth-inhibiting activity, the silver nanoparticle-formed surface was placed in 500 μL of LB medium inoculated with 5 μL of the log-phase-grown *E. coli* cells. For bactericidal activity assay, the silver nanoparticle-formed surface was placed in 500 μL of LB medium containing 1×10^9 cells mL^{-1} *E. coli*. The cells that contacted the silver nanoparticle-formed surfaces were incubated at 37 °C and 300 rpm for 1 day. At the end of incubation period, the culture broth was sampled to count viable bacterial cells. Subsequently, the surfaces were gently washed with DW to remove remaining cells and reincubated, as described above. This process was repeated every day for 7 days and 100 μL of each sampled culture broth was spread onto an LB agar plate. The number of bacterial colony formed on LB plate was counted after incubation overnight at 37 °C. The growth-inhibiting and bactericidal efficacies were calculated using the following formulas, respectively.

$$\text{Growth-inhibiting efficacy (\%)} = (B - A)/B \times 100 \quad (1)$$

$$\text{Bactericidal efficacy (\%)} = (C - A)/C \times 100 \quad (2)$$

Here, A is the number of colony in the sampled culture broth incubated on the surface, B is the number of colony in the sampled culture broth incubated without that surface (control), and C is the initial number of colony in the culture broth applied on the surface.

Cytocompatibility Test. Nontreated bare, nontreated MAP-Ag4-coated, $AgNO_3$-treated bare, and $AgNO_3$-treated MAP-Ag4-coated polystyrene surfaces were used for the cell culture experiments. $AgNO_3$ treatment was performed for 6 days. Each surface was exposed to UV radiation for 2 h and washed three times with DW for 30 min before cell seeding. Mouse preosteoblast MC3T3-E1 cells (RIKEN Cell Bank) were cultured in α-minimal essential medium (α-MEM; HyClone) with 10% (v/v) fetal bovine serum (FBS; HyClone) and penicillin/streptomycin (HyClone) at 37 °C in a humidified atmosphere containing 5% CO_2 and 95% air. All cells were collected by trypsinization and then washed twice in Dulbecco's PBS (DPBS; HyClone). In total, 1×10^4 cells (>95% viable) were seeded on each surface. The cells were allowed to adhere to the surface for 1 h, and unattached cells were washed from the surface by rinsing with DPBS. Then, the attached cells on each surface were incubated in α-MEM supplemented with 10% FBS at 37 °C for 7 days. The amount of cells present after cell attachment and proliferation was quantified by the Cell Counting Kit-8 (CCK-8; Dojindo Laboratories), which uses 2-(2-methoxy-4-nitrophenyl)-3-(4-nitrophenyl)-5-(2,4-disulfophenyl)-2H-tetrazolium (WST-8) to produce a highly water-soluble formazan dye upon reduction in the presence of an electron carrier. The CCK-8 assay was performed after 1 h (attachment) or after 1, 4, or 7 days (proliferation) in α-MEM. For the assay, 25 μL of the CCK-8 solution was added to each well, and the plates were further incubated for 3 h at 37 °C. After incubation, the absorbance was measured at 450 nm using a microplate absorbance spectrophotometer. The viability of MC3T3-E1 cells on the $AgNO_3$-treated MAP-Ag4-coated surface was also measured using the Live/Dead Viability/Cytotoxicity Assay Kit (Invitrogen), which uses calcein AM and ethidium homodimer-1 (EthD-1) as fluorescence dyes and provides simultaneous determination of live and dead cell counts by measuring of intracellular esterase activity and plasma membrane integrity. Live cells show green fluorescence, and dead cells show red fluorescence. The Live/Dead assay was performed after 7 days of incubation in α-MEM; 1 μL of 50 μM calcein AM working solution and 2 μL of 2 mM EthD-1 stock solution were added to each well, and the plates were further incubated for 20 min at 37 °C with protection from light. After incubation, the morphologies of fluorescent cells with fluorescence were observed using an automated fluorescence stereo microscope (Leica).

Mammalian and Bacterial Coculture Experiment. Mouse preosteoblast MC3T3-E1 cells were cultured in the same way as in the cytocompatibility test, except that α-MEM with 10% (v/v) FBS was used without penicillin/streptomycin. 1×10^3 *E. coli* cells mL^{-1} were inoculated into the α-MEM along with the MC3T3-E1 cells. The MC3T3-E1 cells and *E. coli* cells were cocultured for 12 h, after which 100 μL of the culture medium was spread onto an LB agar plate, which was incubated overnight at 37 °C. The colonies grown on the plates were counted in triplicate. The viability of MC3T3-E1 cells on the $AgNO_3$-treated MAP-Ag4-coated surface after coculture with *E. coli* was analyzed using the Live/Dead Viability/Cytotoxicity Assay Kit.

Synthesis of Silver Nanoparticles on Various Surfaces. As a sample surface, pure titanium foil (>99.5% purity; Alfa Aesar) with a thickness of 0.25 mm was cut into 10 × 10 mm pieces, polished using 600 and 1200 grid sandpaper, and ultrasonicated in DW for 30 min. Then, the titanium surface was placed in a piranha solution containing a 4:1 (v/v) mixture of 50% H_2SO_4 and 30% H_2O_2 for 15 min, after which it was rinsed extensively with DW, boiled in DW for 15 min, and then dried under nitrogen gas. Pieces of cover glass (SPL Life Science) with a thickness of 0.10 mm and a diameter of 9 mm and commercial titanium implant abutment (RaphaBio) with a length of 75 mm were also used as sample surfaces. The titanium and glass surfaces were spin-coated with 3 mg mL^{-1} of MAP-Ag4 and incubated with $AgNO_3$ for 6 days.

Fabrication of Silver Nanoparticle-Containing Nanofibers. Solutions for electrospinning were prepared by dissolving polycaprolactone (PCL; M_n = ~80 000; Sigma) and MAP-Ag4 at a concentration of 6 wt % in hexafluoroisopropanol (Sigma). The PCL and MAP-Ag4 solutions were blended with the ratio of 7:3 to obtain composite nanofibers. The blended solution was electrospun using a 5 mL syringe with a needle diameter of 0.4 mm and a mass flow rate of 1 mL h^{-1}. High voltage (13−15 kV) was applied to the tip of the needle attached to the syringe when the fluid jet was ejected. Random nanofibers were collected on flat aluminum foil with a gap distance of 10 cm from the needle tip. Fabricated electrospun nanofibers were vacuum-dried for at least 3 days to enable evaporation of any remaining solvents prior to use. The formation of silver nanoparticles was performed directly by incubating the nanofiber mats in $AgNO_3$ solution.

Statistical Data Analysis. Independent experiments were performed at least 3 times and triplicate samples were analyzed in each experiment. The significance of data obtained with the control and treated groups was statistically analyzed using the paired Student's *t* test.

RESULTS AND DISCUSSION

Construction of MAP-Silver Binding Peptide Fusions. It has been reported that Ag4 (NPSSLFRYLPSD), a silver binding peptide identified by phage display, reduces silver ions to metallic silver without an external reducing agent and binds to silver nanoparticles.[17] Similarly to Ag4, AgP35 (WSWRSPTPHVVT), identified by the polymerase chain reaction (PCR) method, is capable of reducing silver ions to metallic silver.[16] Ag4 and AgP35 peptides have tyrosine (Y) and tryptophan (W) residues, respectively, which have strong electron-donating properties.[38] These amino acid residues might play important roles in reducing silver ions. We genetically fused each of these silver binding peptides to the C-terminus of MAP (Figure 1b), and we confirmed the cloned sequences by direct sequencing. AgNSB (KSLSRHDHIHHH), a nonsilver binding peptide, was used as a control for comparison. For fusion with these different peptides, we used the recombinant hybrid-type MAP, which contains six repeats of type 1 MAP (fp-1) decapeptide at both the N- and C-termini of type 5 MAP (fp-5).[32] In general, it was considered that the adhesive properties of MAPs are involved in the level of L-3,4-dihydroxyphenylalanine (DOPA), which is modified form of tyrosine.[39,40] Macro-scale adhesion strength of MAP increases after enzymatic oxidation of tyrosine residues to DOPA molecules.[37] However, it was experimentally confirmed that recombinant hybrid-type MAP expressed in *E. coli* has significant adhesive and surface coating abilities in microscale even though it is lacked of DOPA and contains original tyrosine residues due to intrinsic inability of *E. coli* to undergo post-translational modification,[32,41] indicating successful utilization of this MAP for surface coating without cumbersome in vitro DOPA modification step. Thus, the unmodified recombinant

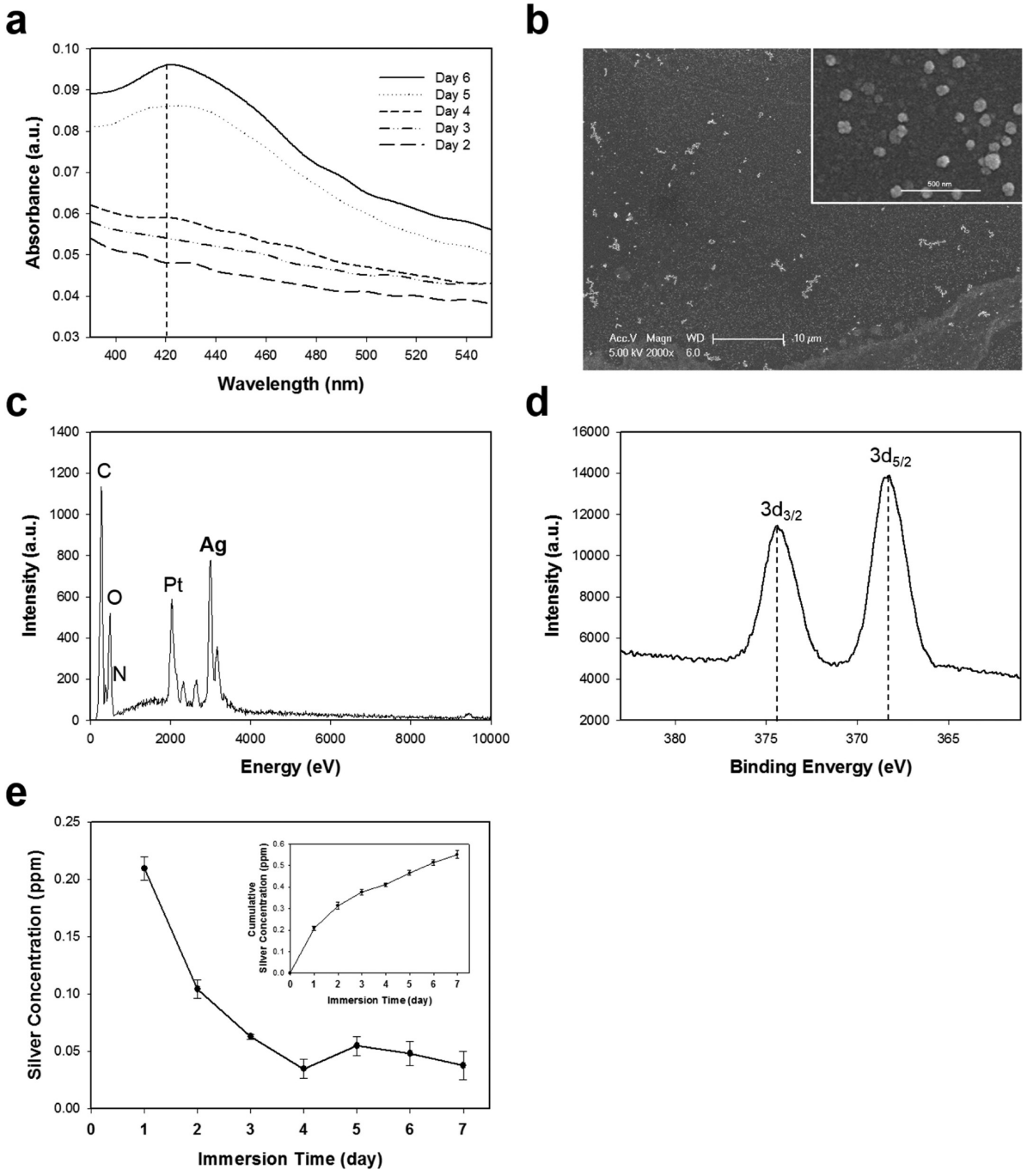

Figure 2. Characterization of silver nanoparticles on $AgNO_3$-treated MAP-Ag4-coated polystyrene surface. (a) UV−vis spectroscopy analysis. (b) Surface morphology examined by SEM. (c) EDS analysis of the elemental composition. (d) XPS analysis of the elemental composition. (e) Noncumulative (outer box) and cumulative silver release (inner box) in physiological environments.

hybrid-type MAP was used in this work because its adhesion strength would be sufficient to effectively interact with silver nanoparticles and bacterial/mammalian cells. The MAP-silver binding peptide fusion proteins were expressed in *E. coli* and purified as previously described.[32−34] Through SDS-PAGE, we confirmed that the MAP fusion proteins (MAP-Ag4, MAP-AgP35, and MAP-AgNSB) were successfully expressed and purified (Figure 1c).

Silver Nanoparticle Formation on MAP-Silver Binding Peptide Fusion-Coated Surfaces. The purified MAP fusion proteins were coated onto polystyrene coverslip surfaces, and the coated surfaces were incubated in a solution of 20 mM $AgNO_3$ to form silver nanoparticles. Generally, silver nanoparticles are known to exhibit size-dependent characteristic surface plasmon resonance absorption peak at approximately 400−440 nm, as measured by UV−vis spectroscopy.[17] We observed a characteristic peak at 420 nm upon incubation of the MAP-Ag4-coated surface in $AgNO_3$ solution (Figure 2a). In the case of the MAP-AgP35-coated surface, a similar peak was observed at 420 nm (Supporting Information Figure S1a). The bare surface and the MAP-AgNSB-coated surface did not generate clear peaks. Interestingly, the original MAP-coated surface without any silver binding peptide moieties showed a relatively clear characteristic peak at 420 nm, although the

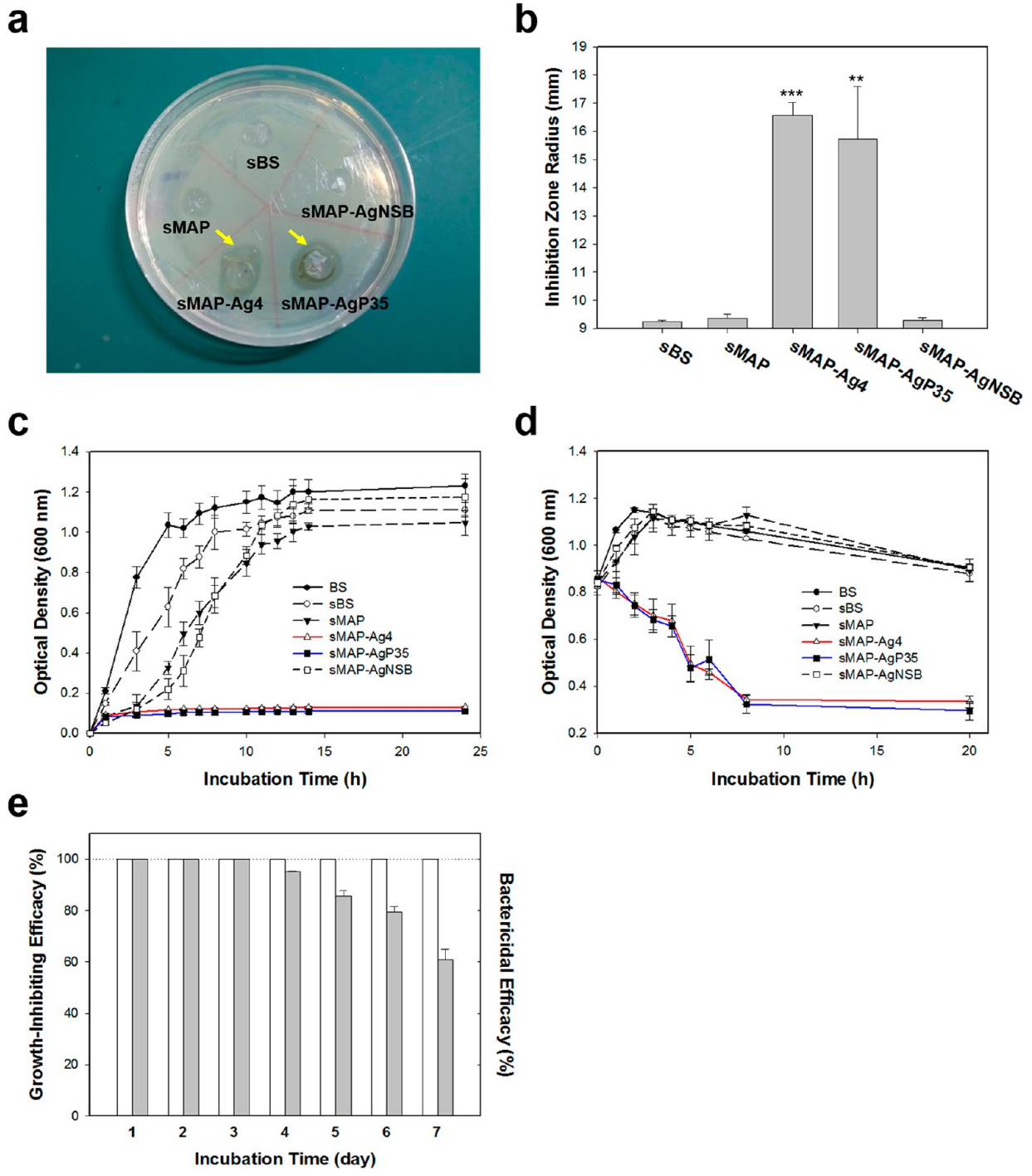

Figure 3. Antibacterial activity of $AgNO_3$-treated MAP-silver binding peptide fusions-coated surfaces against *E. coli*. (a) Disk diffusion test and (b) the diameter of the inhibition zone. Arrows indicate the inhibition zone. The data represent mean ± standard deviation and were analyzed 2-tails student *t* test (*$p < 0.05$, **$p < 0.01$, ***$p < 0.005$). (c) Bacterial growth and (d) bactericidal time profiles for a short period. (e) Growth-inhibiting (white bar) and bactericidal (gray bar) efficacies of $AgNO_3$-treated MAP-Ag4-coated surface for a long period. Abbreviations: BS, nontreated bare surface; sBS, $AgNO_3$-treated bare surface; sMAP, $AgNO_3$-treated MAP-coated surface; sMAP-Ag4, $AgNO_3$-treated MAP-Ag4-coated surface; sMAP-AgP35, $AgNO_3$-treated MAP-AgP35-coated surface; sMAP-AgNSB, $AgNO_3$-treated MAP-AgNSB-coated surface.

intensity of the peak was lower than that of the MAP-Ag4 and MAP-AgP35 fusion proteins, possibly because MAP may adsorb silver ions through its own adhesive property.

SEM analysis revealed the formation of silver nanoparticles on all MAP-silver binding peptide fusion protein-coated surfaces (Figure 2b). We found that the bare surface and the original MAP-coated surface also had some silver nanoparticles attached (Supporting Information Figure S1b). However, there were many morphological differences with regard to the size, shape, population, and distribution of the particles. MAP-Ag4 produced homogeneous small spherical particles with a diameter of approximately 67 ± 7.9 nm, covering a large area (Figure 2b). EDS analysis, which provides a qualitative chemical analysis, confirmed that the nanoparticles synthesized on the MAP-Ag4-coated surface consisted primarily of silver (Figure 2c). Incubation of the MAP-AgP35-coated surface with

$AgNO_3$ also resulted in the formation of small particles with a diameter of approximately 60.2 ± 7.5 nm (Supporting Information Figure S1b), with morphologies similar to those of particles produced on the MAP-Ag4-coated surface. In contrast, the silver nanoparticles formed on the bare, original MAP-coated, and MAP-AgNSB-coated surfaces had different morphologies; they were large, cubical particles with variable particle sizes of 93.7 ± 9.5 nm, 108.6 ± 14.3 nm, and 103.8 ± 12.3 nm, respectively (Supporting Information Figure S1b), and they were also aggregated intermittently and irregularly. It was previously reported that small silver nanoparticles have higher antibacterial activity because of their greater surface area available for interaction with bacterial cells.[42] In addition, silver nanoparticles with highly reactive facets, such as spherical or decahedral particles, have been shown to have efficient bactericidal activity.[43] Therefore, the small size, spherical shape, and homogeneous distribution of the silver nanoparticles generated by MAP-Ag4 and MAP-AgP35 are expected to be favorable for antibacterial applications. The elemental composition of the $AgNO_3$-treated surfaces was also analyzed by XPS. Ag 3d spectra at 374.5 eV (Ag $3d_{3/2}$) and 368.4 eV (Ag $3d_{5/2}$) detected on the MAP-Ag4-coated surface (Figure 2d) corresponded to metallic silver, indicating that the nanoparticles are composed of metallic silver. This finding was consistent with the results obtained by EDS analysis. The Ag 3d doublet around 370 eV was observed on all $AgNO_3$-treated surfaces (Supporting Information Figure S1c), and it was similar to that on the MAP-Ag4-coated surface.

The capacity of our antibacterial coating system to control the amount of silver nanoparticles formed on the MAP-silver binding peptide fusion-coated surface was assessed by varying incubation time in $AgNO_3$ solution or fusion protein concentration in coating solution. As the incubation duration increased, the amount of silver nanoparticles also increased gradually (Supporting Information Figure S2a). However, after 6 days of incubation time, we observed that the size and distribution of silver nanoparticles became heterogeneous and the agglomeration of nanoparticles occurred (Supporting Information Figure S2b), which are both unfavorable for antibacterial applications. The concentration of MAP-silver binding peptide fusion in coating solution was another important factor. The silver nanoparticle formation was increased according to its concentration (Supporting Information Figure S2c), and a large number of smaller, more spherical, and single nanoparticles were formed on the surface coated with higher fusion protein concentration (Supporting Information Figure S2d). These results might be explained by the increase in number of available silver binding peptides according to the increase in protein amount. However, it was previously reported that very small (<10 nm) silver nanoparticles have acute toxicity to mammalian cells as well as high antibacterial activity against bacterial cells.[44] Thus, optimal conditions for preparation of surface-bound silver nanoparticles with appropriate size are important for both effective antibacterial activity and biological safety. The controllable silver nanoparticle formation according to incubation time and protein concentration can be advantageous for practical applications which need balanced amount and size of particles according to usage.

Silver release from the MAP-silver binding peptide fusion-coated polystyrene surface was evaluated. The surface was immersed in physiological solution for up to 7 days with periodic sampling. In general, silver nanoparticles proceed the following redox reaction and release silver ions.[45]

$$2Ag(s) + 1/2O_2(aq) + 2H^+(aq) \leftrightarrow 2Ag^+(aq) + H_2O(aq) \quad (3)$$

Then, the reaction reaches equilibrium, where released silver ions can be recombined in silver nanoparticles when the concentration of released silver ion reaches a certain level. From the silver release time profile, the amount of released silver was relatively high in initial period, but it decreased gradually according to immersion time and reached plateau, with 0.55 ± 0.02 ppm of total cumulative released amount for 7 days (Figure 2e). High initial silver release and diminished afterward release could be appropriate for effective prevention of initial bacterial infection and minimization of toxicity generated by silver ions, respectively.

Antibacterial Activity of Generated Silver Nanoparticles on Coated Surfaces. The antibacterial activity of silver nanoparticles formed on the MAP-silver binding peptide fusion-coated surfaces was first evaluated using the disk diffusion test against different bacteria species. The following Gram-negative bacteria were tested: *E. coli* (Figure 3a, b), *S.* Typhimurium, and *S. dysenteriae*. The Gram-positive bacterium *S. aureus* was also tested (Supporting Information Figure S3). Silver nanoparticles synthesized by MAP-Ag4 and MAP-AgP35 during treatment with $AgNO_3$ solution showed effective antibacterial activity toward all of the tested bacterial strains. The mineralization of the original MAP and MAP-AgNSB resulted in very weak growth inhibition zones for all target strains, and the $AgNO_3$-treated bare surface did not inhibit the growth of *E. coli* (Supporting Information Figure S4). These findings agree with the morphological differences observed by SEM. Additionally, the results highlight the advantages of using an adhesive MAP-silver binding peptide fusion coating to confer an antibacterial effect.

Next, silver nanoparticles synthesized on $AgNO_3$-treated surfaces were incubated in liquid LB media with log-phase *E. coli* (Figure 3c), *S.* Typhimurium, *S. dysenteriae*, or *S. aureus* (Supporting Information Figure S3), and we performed quantitative time profiling of growth-inhibiting activity for a short period of 1 day. The nontreated bare surface was used as another negative control. Both the MAP-Ag4- and MAP-AgP35-coated surfaces inhibited the growth of all target bacterial strains effectively over the course of 24 h, consistent with the results of the disk diffusion test. In addition to showing outstanding growth-inhibiting activities, these coatings presented bactericidal effects against *E. coli* (1×10^9 cells mL^{-1}; Figure 3d). The $AgNO_3$-treated bare, original MAP-coated, and MAP-AgNSB-coated surfaces did not show notable growth-inhibiting and bactericidal activity against *E. coli*, but they showed limited effects against other bacteria, which indicates that efficient antibacterial activity depends on the presence of the silver binding moiety rather than the presence of MAP alone.

Growth-inhibiting and bactericidal efficacies were measured for longer period of 7 days to evaluate sustainability of the silver nanoparticles on the MAP-silver binding peptide fusion-coated surface (Figure 3e). We found that the growth-inhibiting efficacy was perfectly maintained over this time period. The bactericidal efficacy also remained ~100% during the first 3 days, but it decreased gradually afterward. This gradual decrease of bactericidal ability might be caused through silver release to

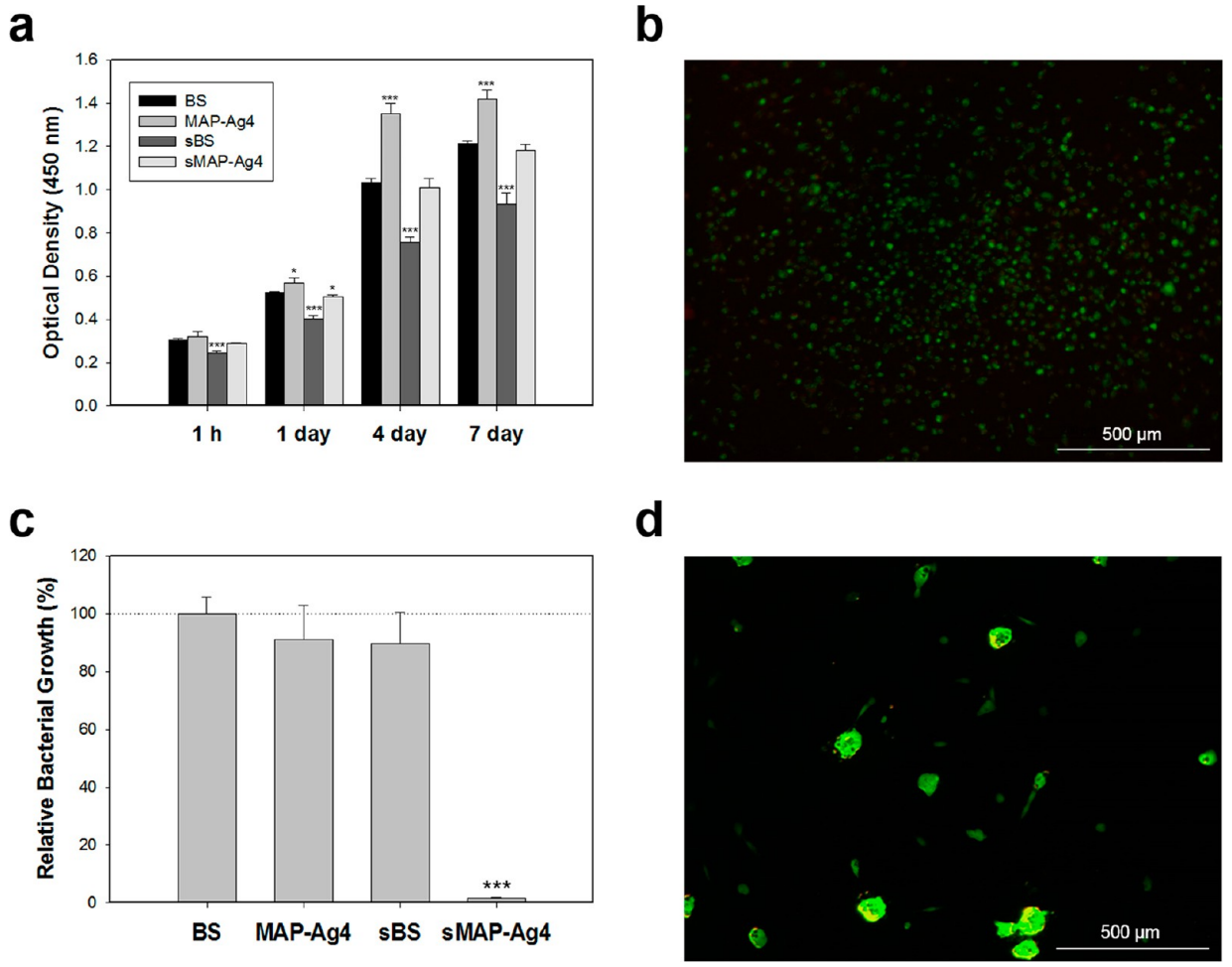

Figure 4. In vitro cytocompatibility test and mammalian/bacterial coculture analysis. (a) Proliferation and (b) viability of sole MC3T3-E1 cells on an $AgNO_3$-treated MAP-Ag4-coated surface. Live cells appear green, whereas dead cells are red. (c) Relative growth of *E. coli* cells grown on LB agar plates after coculture with MC3T3-E1 cells for 12 h. (d) Viability of MC3T3-E1 cells on an $AgNO_3$-treated MAP-Ag4-coated surface in coculture with *E. coli* cells. The data represent mean ± standard deviation and were analyzed 2-tails student *t* test (*$p < 0.05$, **$p < 0.01$, ***$p < 0.005$). Abbreviations: BS, nontreated bare surface; MAP-Ag4, nontreated MAP-Ag4-coated surface; sBS, AgNO3-treated bare surface; sMAP-Ag4, AgNO3-treated MAP-Ag4-coated surface.

some extent in physiological environments (Figure 2e) and/or some inactivated silver nanoparticles being covered by dead bacterial cell-derived proteins and nucleic acids.[46,47] In addition, our bactericidal activity assay employed harsh condition of high bacterial cell density (1×10^9 cells mL^{-1}). In general, it was explained that silver nanoparticles have antibacterial activity either through release of silver ions or through a direct contact-killing mechanism.[48−50] In addition, it was previously reported that surface-bound silver nanoparticles exhibit greater efficacy than colloidal silver nanoparticles.[51] By considering effective growth-inhibiting and bactericidal abilities, we expect that our antibacterial surface coating based on the MAP-silver binding peptide fusions is sustainable for long period in physiological in vivo environments. Sustainable antibacterial activity could help to prevent infection not only right after implant surgery but also during early stage of recovery.

Cytocompatibility of Generated Silver Nanoparticles on Coated Surfaces. We tested in vitro cytocompatibility by using mouse preosteoblast MC3T3-E1 cells to measure cell adhesion and proliferation (Figure 4a). To show unilateral effect of MAP-Ag4 coating and $AgNO_3$ treatment on cell behavior, nontreated MAP-Ag4-coated surface and $AgNO_3$-treated bare surface were used as controls, respectively. The cells on the nontreated MAP-Ag4-coated surface showed higher proliferation rate than that on the nontreated bare surface. It was consistent with the previous result that MAP improves mammalian cell behaviors such as adhesion and proliferation when used as a surface-coating material.[32−34] On the contrary, the proliferation rate of the cells on the $AgNO_3$-treated bare surface was lower than those on all other surfaces including nontreated bare surface. Because it was reported that silver nanoparticles are cytotoxic to various mammalian cells,[52−54] the low proliferation rate on the $AgNO_3$-treated bare surface can be explained. Nevertheless, the cell numbers increased gradually on the $AgNO_3$-treated bare surface in process of culture time because the acute toxic effect of silver nanoparticles appears only at high doses.[55] Cell attachment on the $AgNO_3$-treated MAP-Ag4-coated surface was slightly lower than that on the nontreated bare surface and the MAP-Ag4-coated surface after culturing for 1 h. However, the cells on the $AgNO_3$-treated MAP-Ag4-coated surface showed a proliferation rate comparable to that on the nontreated bare surface. Generally, the cytotoxic effect of silver on mammalian cells may be significantly lower than its antibacterial effect on bacterial cells because eukaryotic cells are usually much larger than prokaryotic cells.[56] In that sense, silver nanoparticles on the

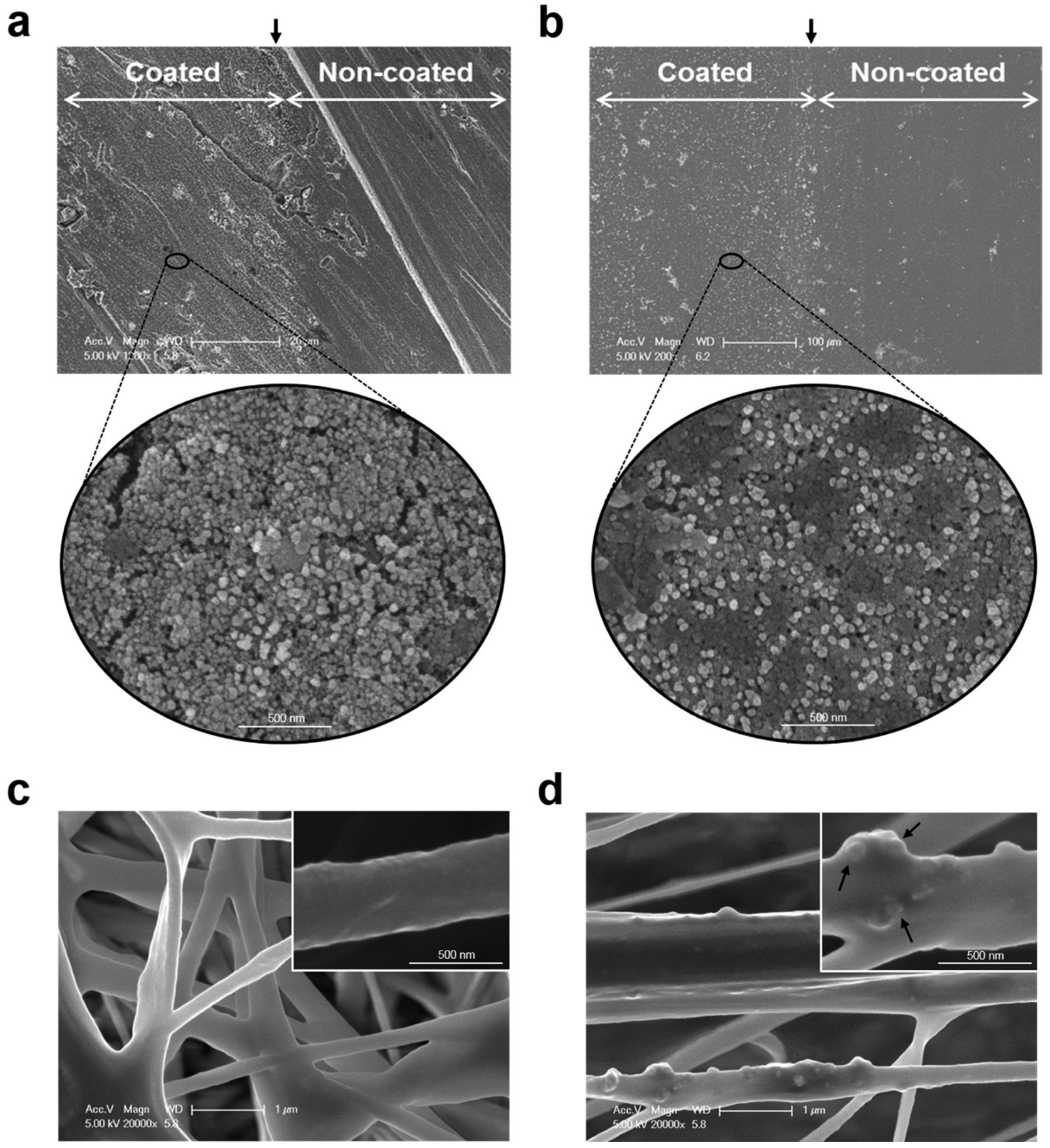

Figure 5. Silver nanoparticle synthesis on titanium, glass, and nanofibers. Silver nanoparticles on $AgNO_3$-treated MAP-Ag4-coated (a) titanium surface and (b) glass surface. Silver nanoparticles were synthesized on only the MAP-Ag4-coated area; they were not synthesized on the noncoated area upon $AgNO_3$ treatment. Black arrows indicate of the boundaries between MAP-Ag4-coated and noncoated areas. (c) Nanofibers fabricated with MAP-Ag4 and (d) silver nanoparticles synthesized on $AgNO_3$-treated MAP-Ag4 nanofibers. Black arrows indicate silver nanoparticles.

$AgNO_3$-treated MAP-Ag4-coated surface are sufficient to destruct bacterial cells without inducing notable cytotoxicity. Furthermore, MAP holds silver nanoparticles not to part from surface and improves mammalian cell behaviors by virtue of its intrinsic properties; thus, these could offset possible cytotoxicity of silver nanoparticles. This hybrid environment incorporating both organic (MAP) and inorganic (silver nanoparticles) phases might lessen the burden of toxicity to mammalian cells. Cell viability on the $AgNO_3$-treated MAP-Ag4-coated surface was also confirmed by fluorescence staining (Figure 4b). After 7 days of incubation, many viable cells (but, few dead cells) were present on the $AgNO_3$-treated MAP-Ag4-coated surface, which is consistent with the results of the proliferation assay. Collectively, the in vitro cell culture assays revealed no notable cytotoxicity of the silver nanoparticles on the $AgNO_3$-treated MAP-Ag4-coated surface.

We sought to comprehensively confirm the observed antibacterial activity and cytocompatibility of the silver nanoparticles on the MAP-Ag4-coated surface under conditions presumed to be similar to those of a biomedical implant after surgery. Preosteoblast MC3T3-E1 cells and *E. coli* cells were cocultured for 1 day, and the remaining *E. coli* cells in the culture medium were spread on an agar plate. The number of *E. coli* colonies formed by the culture sample from the $AgNO_3$-

treated MAP-Ag4-coated surface was significantly lower than that of samples from all other surfaces (Figure 4c), which indicates that the silver nanoparticles on the $AgNO_3$-treated MAP-Ag4-coated surface show strong antibacterial activity toward *E. coli*, even in a coculture environment with mammalian cells. Additionally, fluorescence staining revealed a large number of viable MC3T3-E1 cells on the $AgNO_3$-treated MAP-Ag4-coated surface after coculturing, although the number of viable cells was lower than that in mammalian cell monoculture, and some cell aggregations were observed (Figure 4d). Here, we consider that MAP has important roles with regard to antibacterial activity and cytocompatibility; it enables silver nanoparticles to exhibit antibacterial activity toward bacterial cells intensively and to be immobilized on a restricted space to avoid wandering and harming surrounding mammalian cells. The mammalian and bacterial coculture experiment was used to model an implant surgery accompanied by a bacterial infection. The environment of this experimental model could be representative of mammalian cells in a physiological environment, as the system used MC3T3-E1 cell line having a comparatively high proliferation rate to constantly replace dead cells with new cells.[57] In such a model, it is preferable that the silver nanoparticles inhibit the growth of the bacteria without inhibiting the growth of mammalian cells.

Ideal antibacterial coating materials for medical implants should effectively reduce the bacterial infection rate and be biocompatible with the human body. Our proposed MAP-silver binding peptide fusions not only show excellent antibacterial activity but are also cytocompatible with mammalian cells. Furthermore, they display effective antibacterial activity in an environment in which mammalian cells coexist with bacteria, demonstrating their potential use as antibacterial coating materials for implants in clinical applications.

Silver Nanoparticle Formation on Various Surface Types. In the experiments described above, we showed that silver nanoparticles form successfully on polystyrene plastic surfaces that are coated with MAP-silver-binding peptide fusions. To demonstrate general applicability of the MAP-silver-binding peptide fusion as the surface-independent silver nanoparticle-forming coating material, we tested other surfaces (titanium metal and glass) by coating them with MAP-Ag4 and incubating them in $AgNO_3$ solution. SEM analyses showed that silver nanoparticles were successfully synthesized on all of the tested MAP-Ag4-coated surfaces (Figure 5a, b). Interestingly, the silver nanoparticles that formed on the titanium surface were smaller (approximately half the size) and denser than those on the polystyrene surface. Because the Fermi level of titanium is generally higher than that of silver, electrons move from titanium to silver when silver and titanium are adjacent.[58] The synthesis of silver nanoparticles on a titanium surface followed by coating with MAP-Ag4 and incubation in $AgNO_3$ solution may thus provide an environment that brings silver and titanium atoms into close proximity, which may cause electrons to move from the titanium surface to the silver surface to achieve Fermi level equilibration. Given that titanium is widely used for implant devices, the smaller and denser silver nanoparticles synthesized on titanium surfaces may prove particularly advantageous in terms of their antibacterial activity. Thus, the use of MAP-silver binding peptide fusions for antibacterial coating may be appropriate for titanium-based implant devices. For example, MAP-silver binding peptide fusions could be useful for reducing bacterial colonization and biofilm formation on interspace between titanium implant abutment and crown where easily to be contaminated. We confirmed that MAP-Ag4 was coated on titanium implant abutment surface and synthesized silver nanoparticles successfully (Supporting Information Figure S5). In addition, the MAP-silver binding peptide fusions could be applied to various material surfaces of metal implant devices, such as those made of aluminum, magnesium, or stainless steel.

We also fabricated antibacterial nanofibers based on MAP-Ag4 by electrospinning (Figure 5c). Silver nanoparticles were successfully synthesized on MAP-Ag4 nanofiber surfaces after incubation in $AgNO_3$ solution (Figure 5d). Although some approaches have been reported for functionalization of nanofiber surface by adsorption of silver binding peptide,[59] there was no study on fabrication of nanofibrous scaffolds using silver binding peptide-incorporated biomaterials. Previously, we showed that nanofibers based on MAP can provide a structural backbone for tissue engineering scaffolds with functional bioactive peptides.[35] The MAP-Ag4 nanofibers could also serve as a scaffold for tissue engineering with intrinsic antibacterial activity.

CONCLUSIONS

In the present study, we proposed a novel, simple silver coating method based on recombinant MAP-silver binding peptide fusions. These fusions were constructed by linking silver binding peptide sequences to the C-terminus of MAP, and the resulting fusion proteins made it possible to simply regulate the formation of silver nanoparticles upon incubation with $AgNO_3$ solution. We confirmed that strong adhesion property was conferred by the MAP component, and we showed that the silver binding moiety recruited silver to provide antibacterial property. Moreover, the silver nanoparticles synthesized by MAP-silver binding peptide fusions were confirmed to be cytocompatible. Thus, such coatings have great potential for use in tissue engineering and biomedical applications. Easily applied surface-independent antibacterial coatings on diverse material surfaces and the fabrication of silver nanoparticle-containing nanofibrous scaffolds are good examples of the promising use of the proposed MAP-silver binding peptide fusions.

ASSOCIATED CONTENT

Supporting Information

Experimental results for characterization of silver nanoparticles on $AgNO_3$-treated surfaces; antibacterial activity of $AgNO_3$-treated surfaces against *S.* Typhimurium, *S. dysenteriae*, and *S. aureus*; *E. coli* growth on $AgNO_3$-treated surfaces, information on primers used in the study. This material is available free of charge via the Internet at http://pubs.acs.org.

AUTHOR INFORMATION

Corresponding Author

*E-mail: hjcha@postech.ac.kr.

Author Contributions

[§]Y.K.J. and J.H.S. contributed equally to this work. Y.K.J., J.H.S., and H.J.C. designed the experiments. Y.K.J., B-H.C., B.J.K., and H.H.S performed the experiments. Y.K.J., J.H.S., and B.H.H analyzed the data. H.J.C. supervised the research. Y.K.J., J.H.S., and H.J.C. wrote the manuscript. H.J.C. is the principal investigator.

Notes

The authors declare no competing financial interest.

■ ACKNOWLEDGMENTS

This work was supported by the Marine Biotechnology program (Marine BioMaterials Research Center), funded by the Ministry of Oceans and Fisheries of Korea and the Rising Star program funded by POSTECH.

■ REFERENCES

(1) Costerton, J. W.; Stewart, P. S.; Greenberg, E. P. Bacterial Biofilms: A Common Cause of Persistent Infections. *Science* **1999**, *284*, 1318−1322.
(2) Cen, L.; Neoh, K. G.; Kang, E. T. Gold Nanocrystal Formation on Viologen-Functionalized Polymeric Nanospheres. *Adv. Mater.* **2005**, *17*, 1656−1661.
(3) Pol, V. G.; Srivastava, D. N.; Palchik, O.; Palchik, V.; Slifkin, M. A.; Weiss, A. M.; Gedanken, A. Sonochemical Deposition of Silver Nanoparticles on Silica Spheres. *Langmuir* **2002**, *18*, 3352−3357.
(4) Nie, S.; Emory, S. R. Probing Single Molecules and Single Nanoparticles by Surface-Enhanced Raman Scattering. *Science* **1997**, *275*, 1102−1106.
(5) Dobrovolskaia, M. A.; McNeil, S. E. Immunological Properties of Engineered Nanomaterials. *Nat. Nanotechnol.* **2007**, *2*, 469−478.
(6) Hirano, S. A Current Overview of Health Effect Research on Nanoparticles. *Environ. Health. Prev. Med.* **2009**, *14*, 223−225.
(7) Cioffi, N.; Rai, M. Progress and Prospects. In *Nano-antimicrobials*; Springer-Verlag Publisher: Berlin, Heidelberg, 2012; pp 504.
(8) Monteiro, D. R.; Gorup, L. F.; Takamiya, A. S.; Ruvollo-Filho, A. C.; de Camargo, E. R.; Barbosa, D. B. The Growing Importance of Materials that Prevent Microbial Adhesion: Antimicrobial Effect of Medical Devices Containing Silver. *Int. J. Antimicrob. Agents* **2009**, *34*, 103−110.
(9) Panacek, A.; Kvitek, L.; Prucek, R.; Kolar, M.; Vecerova, R.; Pizurova, N.; Sharma, V. K.; Nevecna, T.; Zboril, R. Silver Colloid Nanoparticles: Synthesis, Characterization, and Their Antibacterial Activity. *J. Phys. Chem. B* **2006**, *110*, 16248−16253.
(10) Taglietti, A.; Arciola, C. R.; D'Agostino, A.; Dacarro, G.; Montanaro, L.; Campoccia, D.; Cucca, L.; Vercellino, M.; Poggi, A.; Pallavicini, P.; Visai, L. Antibiofilm Activity of a Monolayer of Silver Nanoparticles Anchored to an Amino-Silanized Glass Surface. *Biomaterials* **2014**, *35*, 1779−1788.
(11) Li, Z.; Lee, D.; Sheng, X.; Cohen, R. E.; Rubner, M. F. Two-Level Antibacterial Coating with Both Release-Killing and Contact-Killing Capabilities. *Langmuir* **2006**, *22*, 9820−9823.
(12) Oloffs, A.; Grosse-Siestrup, C.; Bisson, S.; Rinck, M.; Rudolph, R.; Gross, U. Biocompatibility of Silver-Coated Polyurethane Catheters and Silver-Coated Dacron Material. *Biomaterials* **1994**, *15*, 753−758.
(13) Liao, Y.; Wang, Y.; Feng, X.; Wang, W.; Xu, F.; Zhang, L. Antibacterial Surfaces through Dopamine Functinoalization and Silver Nanoparticle Immobilization. *Mater. Chem. Phys.* **2010**, *121*, 534−540.
(14) Vaidyanathan, R.; Kalishwaralal, K.; Gopalram, S.; Gurunathan, S. Nanosilver—The Burgeoning Therapeutic Molecule and Its Green Synthesis. *Biotechnol. Adv.* **2009**, *27*, 924−937.
(15) Dahl, J. A.; Maddus, B. L. S.; Hutchison, J. E. Toward Greener Nanosynthesis. *Chem. Rev.* **2007**, *107*, 2228−2269.
(16) Naik, R. R.; Jones, S. E.; Murray, C. J.; McAuliffe, J. C.; Vaia, R. A.; Stone, M. O. Peptide Templates for Nanoparticle Synthesis Derived from Polymerase Chain Reaction-Driven Phage Display. *Adv. Funct. Mater.* **2004**, *14*, 25−30.
(17) Naik, R. R.; Stringer, S. J.; Agarwal, G.; Jones, S. E.; Stone, M. O. Biomimetic Synthesis and Patterning of Silver Nanoparticles. *Nat. Mater.* **2002**, *1*, 169−172.
(18) Brown, S.; Sarikaya, M.; Johnson, E. A Genetic Analysis of Crystal Growth. *J. Mol. Biol.* **2000**, *299*, 725−735.
(19) Cha, J. N.; Stucky, G. D.; Morse, D. E.; Deming, T. J. Biomimetic Synthesis of Ordered Silica Structures Mediated by Block Copolypeptides. *Nature* **2000**, *403*, 289−292.
(20) Douglas, T.; Strable, E.; Willits, D.; Aitouchen, A.; Libera, M.; Young, M. Protein Engineering of a Viral Cage for Constrained Nanomaterials Synthesis. *Adv. Mater.* **2002**, *14*, 415−418.
(21) Dickerson, M. B.; Sandhage, K. H.; Naik, R. R. Protein- and Peptide-Directed Syntheses of Inorganic Materials. *Chem. Rev.* **2008**, *108*, 4935−4978.
(22) Gurunathan, S.; Kalishwaralal, K.; Vaidyanathan, R.; Venkataraman, D.; Ram Kumar Pandian, S.; Muniyandi, J.; Hariharan, N.; Eom, S. H. Biosynthesis, Purification and Characterization of Silver Nanoparticles Using *Escherichia coli*. *Colloids Surf., B* **2009**, *74*, 328−335.
(23) Deepak, V.; Umamaheshwaran, P. S.; Guhan, K.; Nanthini, R. A.; Krithiga, B.; Jaithoon, N. M. H.; Gurunathan, S. Synthesis of Gold and Silver Nanoparticles Using Purified URAK. *Colloids Surf., B* **2011**, *86*, 353−358.
(24) Lee, E.; Kim, D.-H.; Woo, Y.; Hur, H.-G.; Lim, Y. Solution Structure of Peptide AG4 Used to From Silver Nanoparticles. *Biochem. Biophys. Res. Commun.* **2008**, *376*, 595−598.
(25) Xu, Z.; Jinchun, C.; Peng, Y.; Wantai, Y. Biomimetic Synthesis Silver Crystallite by Peptide AYSSGAPPMPPF Immobilize on PET Film In Vitro. *J. Inorg. Biochem.* **2005**, *99*, 1692−1697.
(26) Xu, Z.; Peng, Y.; Wantai, Y.; Jinchun, C. The Bio-Inspired Approach to Controllable Biomimetic Synthesis of Silver Nanoparticles in Organic Matrix of Chitosan and Silver-Binding Peptide (NPSSLFRYLPSD). *Mater. Sci. Eng. C* **2008**, *28*, 237−242.
(27) Fullenkamp, D. E.; Rivera, J. G.; Gong, Y.; Lau, K. H. A.; He, L.; Varshney, R.; Messersmith, P. B. Mussel-Inspired Silver-Releasing Antibacterial Hydrogels. *Biomaterials* **2012**, *33*, 3783−3791.
(28) Black, K. C. L.; Liu, Z.; Messersmith, P. B. Catechol Redox Induced Formation of Metal Core−Polymer Shell Nanoparticles. *Chem. Mater.* **2011**, *23*, 1130−1135.
(29) Sureshkumar, M.; Siswanto, D. Y.; Chen, Y.-C.; Lee, C.-K.; Wang, M.-J. Antibacterial and Biocompatible Surfaces Based on Dopamine Autooxidized Silver Nanoparticles. *J. Polym. Sci., Part B: Polym. Phys.* **2013**, *51*, 303−310.
(30) Dove, J.; Sheridan, P. Adhesive Protein from Mussels: Possibilities for Dentistry, Medicine, and Industry. *J. Am. Dent. Assoc., JADA* **1986**, *112*, 879.
(31) Waite, J. H.; Tanzer, M. L. Polyphenolic Substance of *Mytilus edulis*: Novel Adhesive Containing L-Dopa and Hydroxyproline. *Science* **1981**, *212*, 1038−1040.
(32) Hwang, D. S.; Gim, Y.; Yoo, H. J.; Cha, H. J. Practical Recombinant Hybrid Mussel Bioadhesive fp-151. *Biomaterials* **2007**, *28*, 3560−3568.
(33) Hwang, D. S.; Sim, S. B.; Cha, H. J. Cell Adhesion Biomaterial Based on Mussel Adhesive Protein Fused with RGD Peptide. *Biomaterials* **2007**, *28*, 4039−4046.
(34) Choi, B.-H.; Choi, Y. S.; Kang, D. G.; Kim, B. J.; Song, Y. H.; Cha, H. J. Cell Behavior on Extracellular Matrix Mimic Materials Based on Mussel Adhesive Protein Fused with Functional Peptides. *Biomaterials* **2010**, *31*, 8980−8988.
(35) Kim, B. J.; Choi, Y. S.; Cha, H. J. Reinforced Multifunctionalized Nanofibrous Scaffolds Using Mussel Adhesive Proteins. *Angew. Chem., Int. Ed.* **2012**, *51*, 675−678.
(36) Lim, S.; Choi, Y. S.; Kang, D. G.; Song, Y. H.; Cha, H. J. The Adhesive Properties of Coacervated Recombinant Hybrid Mussel Adhesive Proteins. *Biomaterials* **2010**, *31*, 3715−3722.
(37) Bauer, A. W.; Kirby, W. M. M.; Sherries, J. C.; Tuck, M. Antibiotic Susceptibility Testing by a Standardized Disc Diffusion Method. *Am. J. Clin. Pathol.* **1966**, *45*, 493−496.
(38) Si, S.; Mandal, T. K. Tryptophan-Based Peptides to Synthesize Gold and Silver Nanoparticles: A Mechanistic and Kinetic Study. *Chem.—Eur. J.* **2007**, *13*, 3160−3168.
(39) Yu, M. E.; Deming, T. J. Synthetic Polypeptide Mimics of Marine Adhesives. *Macromolecules* **1998**, *31*, 4739−4745.
(40) Yu, M. E.; Hwang, J. Y.; Deming, T. J. Role of L-3,4-Dihydroxyphenylalanine in Mussel Adhesive Proteins. *J. Am. Chem. Soc.* **1999**, *121*, 5825−5826.

(41) Cha, H. J.; Hwang, D. S.; Lim, S.; White, J. D.; Matos-Perez, C. R.; Wilker, J. J. Bulk Adhesive Strength of Recombinant Hybrid Mussel Adhsive Protein. *Biofouling* **2009**, *25*, 99−107.
(42) Pal, S.; Tak, Y. K.; Song, J. M. Does the Antibacterial Activity of Silver Nanoparticles Depend on the Shape of the Nanoparticle? A Study of the Gram-negative Bacterium *Escherichia coli*. *Appl. Environ. Microbiol.* **2007**, *73*, 1712−1720.
(43) Morones, J. R.; Elechiguerra, J. L.; Camacho, A.; Holt, K.; Kouri, J. B.; Ramirez, J. T.; Yacaman, M. J. The Bactericidal Effect of Silver Nanoparticles. *Nanotechnology* **2005**, *15*, 2346−2353.
(44) Gliga, A.; Skoglund, S.; Odnevall Wallinder, I.; Fadeel, B.; Karlsson, H. L. Size-Dependent Cytotoxicity of Silver Nanoparticles in Human Lung Cells: The Role of Cellular Uptake, Agglomeration, and Ag Release. *Part. Fibre. Toxicol.* **2014**, *11*, 11−27.
(45) Liu, J.; Hurt, R. H. Ion Release Kinetics and Particle Persistence in Aqueous Nano-Silver *Colloids*. *Environ. Sci. Technol.* **2010**, *44*, 2169−2175.
(46) Pinto, R. J. B.; Marques, P. A. A. P.; Neto, C. P.; Trindade, T.; Daina, S.; Sadocco, P. Antibacterial Activity of Nanocomposites of Silver and Bacterial or Vegetable Cellulosic Fibers. *Acta Biomater.* **2009**, *5*, 2279−2289.
(47) Maneerung, T.; Tokura, S.; Rujiravanit, R. Impregnation of Silver Nanoparticles into Bacterial Cellulose for Antimicrobial Wound Dressing. *Carbohydr. Polym.* **2008**, *72*, 43−51.
(48) Ho, C. H.; Tobis, J.; Sprich, C.; Thomann, R.; Tiller, J. C. Nanoseparated Polymeric Networks with Multiple Antimicrobial Properties. *Adv. Mater.* **2004**, *16*, 957−961.
(49) Sambhy, V.; MacBride, M. M.; Peterson, B. R.; Sen, A. Silver Bromide Nanoparticle/Polymer Composites: Dual Action Tunable Antimicrobial Materials. *J. Am. Chem. Soc.* **2006**, *128*, 9798−9808.
(50) Woodyard, L. L.; Bowersock, T. L.; Turek, J. J.; McCabe, G. P.; Deford, J. A Comparison of the Effects of Several Silver-Treated Intravenous Catheters on the Survival of Staphylococci in Suspension and Their Adhesion to the Catheter Surface. *J. Controlled Release* **1996**, *40*, 23−30.
(51) Agnihotri, S.; Mukherji, S.; Mukherji, S. Immobilized Silver Nanoparticles Enhance Contact Killing and Show Highest Efficacy: Elucidation of the Mechanism of Bactericidal Action of Silver. *Nanoscale* **2013**, *5*, 7328−7340.
(52) Hussain, S. M.; Hess, K. L.; Gearhart, J. M.; Geiss, K. T.; Schlager, J. J. In Vitro Toxicity of Nanoparticles in BRL 3A Rat Liver Cells. *Toxicol. In Vitro* **2005**, *19*, 975−983.
(53) Moaddab, S.; Ahari, H.; Shahbazzadeh, D.; Motallebi, A. A.; Anvar, A. A.; Rahnman-Nya, J.; Shokrgozar, M. R. Toxicity Study of Nanosilver (Nanocid) on Osteoblast Cancer Cell Line. *Int. Nano. Lett.* **2011**, *1*, 11−16.
(54) Kim, S.; Choi, J. E.; Choi, J.; Chung, K.-H.; Park, K.; Yi, J.; Ryu, D.-Y. Oxidative Stress-Dependent Toxicity of Silver Nanoparticles in Human Hepatoma Cells. *Toxicol. In Vitro* **2009**, *23*, 1076−1084.
(55) Kawata, K.; Osawa, M.; Okabe, S. In Vitro Toxicity of Silver Nanoparticles at Noncytotoxic Doses to HepG2 Human Hapatoma Cells. *Environ. Sci. Technol.* **2009**, *43*, 6046−6051.
(56) Alt, V.; Bechert, T.; Steinrucke, P.; Wagener, M.; Seidel, P. An In Vitro Assessment of the Antibacterial Properties and Cytotoxicity of Nanoparticulate Silver Bone Cement. *Biomaterials* **2004**, *25*, 4383−4391.
(57) Towler, D. A.; Arnaud, R. S. Use of Cultured Osteoblastic Cells to Identify and Characterize Transcriptional Regulatory Complexes. In *Principles of Bone Biology*, 3rd ed.; Bilezikian, J. P., Raisz, L. G., Rodan, G. A., Eds.; Academic Press: San Diego, CA, 2008; p 1506.
(58) Rao, K. V. S.; Lavedrine, B.; Boule, P. Influence of Metallic Species on TiO_2 for the Photocatalytic Degradation of Dyes and Dye Intermediates. *J. Photochem. Photobiol., A* **2003**, *154*, 189−193.
(59) Yu, L.; Banerjee, I. A.; Matsui, H. J. Direct Growth of Shape-Controlled Nanocrystals on Nanotubes via Biological Recognition. *J. Am. Chem. Soc.* **2003**, *125*, 14837−14840.